Optimization of Wall Electrodes for Electro-Hydrodynamic Control of Natural Convection During Solidification

Marcelo J. Colaço[1], George S. Dulikravich[2], Thomas J. Martin[3]

[1] Department of Mechanical Engineering, EE/COPPE, Federal University of Rio de Janeiro, UFRJ; Cid Universitaria, Cx. Postal 68503, Rio de Janeiro, RJ, 21945-970, Brazil

[2]Department of Mechanical and Materials Engineering, Florida International University, 10555 West Flagler Street, Miami, FL 33174, USA

[3]Pratt & Whitney Engine Company, Turbine Discipline Engineering & Optimization Group; 400 Main Street, M/S 169-20; East Hartford, CT 06108, USA

This is a **revised** version of manuscript no. **MPP 23-364**. Send all correspondence to:

George S. Dulikravich, Professor and Chairperson
Florida International University
College of Engineering, Room EC 3474
Department of Mechanical and Materials Engineering
10555 West Flagler Street
Miami, Florida 33174
(305) 348-7016 (phone)
(305) 348-6007 (FAX)
dulikrav@fiu.edu (E-mail)

ABSTRACT

This paper presents a numerical procedure to reduce and possibly control the natural convection effects in a cavity filled with a molten material by applying an external electric field whose intensity and spatial distributions are obtained by the use of a hybrid optimizer.

In the case of steady electro-hydrodynamics (EHD), the flow-field of electrically charged particles in a solidifying melt is influenced by an externally applied electric field while the existence of any magnetic field is neglected. Solidification front shape, distribution of the charged particles in the accrued solid, and the amount of accrued solid phase in such processes can be influenced by an appropriate distribution and orientation of the electric field.

The transient Navier-Stokes and Maxwell equations were discretized using the finite volume method in a generalized curvilinear non-orthogonal coordinate system. For the phase change problems, we used the enthalpy method. Variation of intensities of electric potentials on the electrodes along the boundaries of the cavity were described using B-splines. The inverse problem was then formulated to find the electric boundary conditions (the coefficients of the B-splines) in such a way that the gradients of temperature along the horizontal direction are minimized. For this task we used a hybrid optimization algorithm which incorporates automatic switching among several of the most popular optimization modules; the Davidon-Fletcher-Powell (DFP) gradient method, a genetic algorithm (GA), the Nelder-Mead (NM) simplex method, quasi-Newton algorithm of Pshenichny-Danilin (LM), differential evolution (DE), and sequential quadratic programming (SQP).

The optimization results have shown that it is possible to control the natural convection phenomena by using an externally applied electric field. This conceptually new approach to manufacturing could be used in creation of layered and functionally graded material objects.

NOMENCLATURE

b	electric mobility
C_P	specific heat at constant pressure
D_e	electric diffusion coefficient
E	electric field vector
E_x	electric field component in *x*-direction
E_y	electric field component in *y*-direction
g	acceleration of the gravity
f	solid fraction
J	electric current density vector
k	partition coefficient
K	thermal conductivity
L	latent heat of solidification/melting
h	enthalpy
P	pressure
q_e	local free electric charge per unit volume
Ra	Rayleigh number
t	time
T	temperature
u	velocity component in *x*-direction
v	velocity component in *y*-direction
x, *y*	Cartesian coordinates

Greek letters

α thermal diffusivity

β thermal expansion coefficient

ε_0 vacuum dielectric constant or electric permittivity

φ electric potential

μ fluid viscosity

σ electric conductivity

Subscripts

h hot surface

c cold surface

l liquid value

m melting value

s solid value

0 reference value

INTRODUCTION

During solidification from a melt, if the control of melt motion is performed exclusively via an externally applied variable temperature field, it will take quite a long time for the thermal front to propagate throughout the melt eventually causing local melt density variations and altering the thermal buoyancy forces. It has been well known that an externally applied steady magnetic or electric field can, almost instantaneously, influence the flow-field vorticity and change the flow pattern in an electrically conducting fluid [1]. Due to the complexity of the combined electro-magneto-hydro-dynamic (EMHD) mathematical model [2], the EMHD has traditionally been treated as a separate magneto-hydro-dynamic (MHD) sub-model [3] or a separate electro-magneto-hydro-dynamic (EHD) sub-model [3].

A steady state version of EHD solidification analysis without any optimization was studied and published already [4]. However, in the current work we developed a computer code that is capable of simulating transient EHD flows with phase change. The objective of this work is to combine this electrohydrodynamic analysis and an optimization study [5] in order to minimize the natural convection effects in a cavity filled with a molten material. By minimizing the natural convection effects, it is possible to produce materials with lower thermal stresses and lower amount of impurities than those obtained in the presence of very strong buoyancy forces.

We treated electrodes on the walls of the container as having continuously varying electric field potential. An appropriate variation of the electric potential along the wall electrodes was then determined by using a hybrid optimization algorithm with the objective of minimizing a certain measure (objective function or cost function) quantifying the intensity of local melt flow-field.

Potential applicability of this concept is very broad in the general field of manufacturing new functionally graded non-isotropic materials and objects with preferred and vastly different capabilities to deform and conduct electricity and heat in different directions. Since the entire simulation algorithm is time-dependent, the basic concept could be reformulated in the future as an optimal control problem where the intensity variation of the electric field along the boundaries of the solidification container can be also varied in time. This way, desired additives or dopants could be injected and deposited at the desired locations in the advancing solidification front thus creating a truly functionally graded material with *a priori* specified spatial variation of physical properties and possibly a prescribed variation of microstructure [6].

This entire concept is applicable to any molten material that has reasonable electric conductivity, either inherent or because it contains at least a small amount of metal, salts or electrically charged particles. One such material is gallium arsenide. It is an important material in electronics industry [7,8]. Other obvious applications could involve controlled solidification of aluminum melts, molten steel superalloys, or electropolymers. Notice that the EHD principle discussed in this paper offers advantages of lower weight and simpler application in an industrial setting than its MHD counterpart [9-13]. Notice also that this new general manufacturing concept does not create only enhanced electromagnetic stirring of the melt [14]. Instead, it offers a possibility of smart manufacturing of solidification products provided by optimally controlled segmented wall electrodes.

Two test cases are presented in this proof-of-the-concept paper. The first involves only natural convection. The second involves phase change in the presence of a natural convection. Applying an optimized electric field obtained by the use of a hybrid optimizer reduced the natural convection effects.

DIRECT PROBLEM

The physical problem considered here involves the laminar electrohydrodynamic natural convection of an incompressible Newtonian fluid. The fluid physical properties are assumed constant within each phase (solid or liquid) and linearly varying in the mushy region between the two phases. The energy source term resulting from viscous dissipation is neglected and buoyancy effects are approximated by the Boussinesq hypothesis. Then the Maxwell and Navier-Stokes equations for a quasi-static electric field system can be written, for the Cartesian coordinate system as [1]

$$\nabla \cdot (\varepsilon_0 \mathbf{E}) = q_e \qquad (1.a)$$

$$\nabla \times \mathbf{E} = 0 \qquad (1.b)$$

$$\frac{\partial q_e}{\partial t} + \nabla \cdot \mathbf{J} = 0 \qquad (1.c)$$

$$\nabla \cdot \mathbf{v} = 0 \qquad (2.a)$$

$$\rho \frac{D\mathbf{v}}{Dt} = -\rho \mathbf{g}[1 - \beta(T - T_0)] - \nabla P + \nabla \cdot \left[\mu\left(\nabla \mathbf{v} + \nabla \mathbf{v}^T\right)\right] + q_e \mathbf{E} \qquad (2.b)$$

$$\rho C_P \frac{DT}{Dt} = \nabla \cdot [K \nabla T] + \mathbf{J} \cdot \mathbf{E} \qquad (2.c)$$

Under the action of the electrical field, the charge carriers of mobility *b* migrate with a velocity *b*E, E being the field modified by the space-charge density q_e. If v is the fluid velocity, then the total current is [1]

$$\mathbf{J} = q_e (b\mathbf{E} + \mathbf{v}) \qquad (3)$$

if the diffusion current is neglected. The latter has the form $-D_e \nabla q_e$ if D_e is the diffusion coefficient. If we deal with electric fields in the 10^4 to 10^5 volts cm^{-1} range, this will be very small, except when gradients occur over lengths of the order less than 10^{-6} cm [1].

Since the electric field is irrotational, according to equation (1.b), it follows that

$$\mathbf{E} = -\nabla \varphi \qquad (4)$$

where φ is the electric potential. Thus, from equation (1.a), we have

$$\nabla^2 \varphi = -\frac{q_e}{\varepsilon_0} \qquad (5)$$

The complete system of Navier-Stokes and Maxwell equations can be written then as

$$\frac{\partial Q}{\partial t} + \frac{\partial E}{\partial x} + \frac{\partial F}{\partial y} = S \qquad (6)$$

where

$$Q = \lambda \phi \qquad (7.a)$$

$$E = (\lambda u + \zeta E_x)\phi^* - \Gamma \frac{\partial \phi^{***}}{\partial x} \qquad (7.b)$$

$$F = (\lambda v + \zeta E_y)\phi^{**} - \Gamma \frac{\partial \phi^{***}}{\partial y} \qquad (7.c)$$

The values of S, λ, ζ, ϕ, ϕ^*, ϕ^{**},ϕ^{***} and Γ are given in Table 1 for the equations of conservation of mass, *x*-momentum, *y*-momentum, energy, electric potential and electric charged particles distribution.

Table 1. Parameters for the Navier-Stokes and Maxwell equations

Conservation of	λ	ζ	ϕ	ϕ*	ϕ**	ϕ***	Γ	S
Mass	ρ	0	1	1	1	1	0	0
x-momentum	ρ	0	u	u	u	u	μ	$-\dfrac{\partial P}{\partial x}+q_e E_x$
y-momentum	ρ	0	v	v	v	v	μ	$-\dfrac{\partial P}{\partial y}-\rho g\left[1-\beta\left(T-T_0\right)\right]+q_e E_y$
Energy	ρ	0	h	h	h	T	K	$C_P\left[b\left(E_x^2+E_y^2\right)+uE_x+vE_y-D_e\left(E_x\dfrac{\partial q_e}{\partial x}+E_y\dfrac{\partial q_e}{\partial y}\right)\right]$
Electric potential	0	0	0	0	0	φ	1	$-\dfrac{q_e}{\varepsilon_0}$
Electric charged particles distribution	1	b	q_e	q_e	q_e	q_e	D_e	0

Note that we used the Boussinesq approximation for the variation of the density with temperature in the *y*-momentum conservation equation. Also note that in the energy conservation equation, the term C_PT was replaced by the enthalpy, *h*, per unit mass. This is useful for problems dealing with phase change where we used the enthalpy method [15]. Admittedly, the actual physics of the binary mixture solidification is more complicated and this physics could be more adequately modeled by using more advanced and complete models [16-18]. However, the objective here was not to develop a more advanced mathematical model of solidification. Instead, our focus was on demonstrating feasibility of a novel concept of controlling solidifying melt flows via externally applied electric fields. Refined and more complete mathematical models [16-18] could be implemented relatively easily once the basic concept has been demonstrated.

The above equations were transformed from the physical to the body-fitted coordinate system (ξ,η) and solved by the finite volume method. The SIMPLEC Method [19] was used to solve the velocity-pressure coupling problem. The WUDS interpolation scheme [20] was used to obtain the values of u, v, h, φ and q_e as well as their derivatives at the interfaces of each control volume. The resulting linear system was solved by the GMRES method [21].

PHASE-CHANGE MODEL

In this paper we used the enthalpy method [15] to deal with the phase change problem. In this method, the energy equation appears as a mixed enthalpy-temperature equation. Thus, we must obtain some relationship between the temperature and the enthalpy to be used in the energy equation.

For the case of a binary alloy, if $h < h_{\text{solid}}$, we have:

$$T = \frac{h}{C_{Ps}} \qquad (8.a)$$

or, if $h > h_{\text{liquid}}$:

$$T = \frac{h + T_s\left(C_{Pl} - C_{Ps} - L\right)}{C_{Pl}} \qquad (8.b)$$

or yet, if $h_{\text{solid}} < h < h_{\text{liquid}}$:

$$T = T_s = T_l = T_{melt} \qquad (8.c)$$

For the mixture, we have a range of temperatures where solidification might occur. Then, if $h_{\text{solid}} < h < h_{\text{liquid}}$,

$$T = \frac{h + \left[T_s\left(C_{Pl} - C_{Ps}\right) - L\right]\left(1 - f\right)}{C_{Pl} + f\left(C_{Ps} - C_{Pl}\right)} \tag{9}$$

where the solid fraction f is given by the Scheil's model [6]:

$$f = 1 - \left(\frac{T_s - T}{T_s - T_l}\right)^{1/(k-1)} \tag{10}$$

In the above equation, we set the partition coefficient $k = 2$, which reduces the Scheil's model to the linear interpolation function. Note that if $T < T_{\text{solid}}$, f must be set to unity and, if $T > T_{\text{liquid}}$, f must be set to zero.

The electric and thermal properties were approximated as linear functions within the mushy region ($T_{\text{solid}} < T < T_{\text{liquid}}$) and kept constant within each phase. Thus, in the mushy region

$$\psi = f\psi_s + \left(1 - f\right)\psi_l \tag{11}$$

where ψ represents the density, thermal conductivity, viscosity, electric mobility and electric conductivity. For the viscosity of the solid phase we used

$$\frac{\mu_s}{\mu_l} \geq 10^5 \tag{12}$$

and for the specific heat at constant pressure within the mushy region, we used the thermodynamic property

$$C_P = \frac{\partial h}{\partial T} \approx \frac{\sqrt{\left(\frac{\partial h}{\partial x}\right)^2 + \left(\frac{\partial h}{\partial y}\right)^2}}{\sqrt{\left(\frac{\partial T}{\partial x}\right)^2 + \left(\frac{\partial T}{\partial y}\right)^2}} \tag{13}$$

Note that, if we are dealing with a mixture, the enthalpy is a function of the temperature, which is a function of the solid fraction, which is itself a function of the temperature. Thus, if $h_{\text{solid}} < h < h_{\text{liquid}}$, we must solve a non-linear system for T. From Eqs. (9) and (10) we have:

$$\frac{T - h + \left[T_s\left(C_{Pl} - C_{Ps}\right) - L\right]\left[\left(\frac{T_s - T}{T_s - T_l}\right)^{1/(k-1)}\right]}{C_{Pl} + \left[1 - \left(\frac{T_s - T}{T_s - T_l}\right)^{1/(k-1)}\right]\left(C_{Ps} - C_{Pl}\right)} = 0 \tag{14}$$

which can be solved, for example, by the secant method.

HYBRID OPTIMIZATION APPROACH

The hybrid optimization algorithm [5, 11-13, 22] utilized in this work incorporates some of the most popular optimization algorithms: genetic algorithm, a quasi-Newton method, modified Nelder-Mead simplex method, sequential quadratic programming, Davidon-Fletcher-Powell gradient search algorithm and differential evolution. Each technique provides a unique approach to optimization with varying degrees of convergence, reliability and robustness at different cycles during the iterative optimization procedure. A set of analytically formulated rules and switching criteria were coded into the program to automatically switch back and forth among the different optimization algorithms as the iterative minimization process proceeded [5].

The evolutionary hybrid algorithm handles the existence of equality and inequality constraint functions in three ways: Rosen's projection method, feasible searching, and random design generation. Rosen's projection method provided search directions that guided descent-directions tangent to active constraint boundaries. In the feasible search, designs that violated constraints were automatically restored to feasibility via the minimization of the active global constraint functions. If at any time this constraint minimization failed, random designs were generated about the current design until a new feasible design was reached.

Gradients of the objective and constraint functions with respect to the design variables, also called design sensitivities, were calculated using finite differencing formulas. The population matrix was updated every iteration with new designs and ranked according to the value of the objective function. During the optimization process, local minima can occur and halt the process before achieving an optimal solution. In this case, the optimizer switches to another method. The user can also stop the iterative process, switch manually to another method and restart the optimizer from the previous iteration.

The population matrix was updated every iteration with new designs and ranked according to the value of the objective function. The optimization problem was completed when the maximum number of iterations or objective function evaluations were exceeded, or when the optimization program tried all individual optimization algorithms and failed to produce a non-negligible decrease in the objective function (which was set at 10^{-4}). Since the value of the global minimum and how many local minimums exist are not known *a priori*, the first criterion was the primary qualification of convergence, indicating that no other minimum could be found.

INVERSE PROBLEM OF DETERMINING THE UNKNOWN ELECTRIC FIELD BOUNDARY CONDITIONS

In this paper we deal with the inverse determination of the electric boundary conditions that create some pre-specified flow-field within some region [11-13, 22]. Figure 1 shows the geometry and the boundary conditions for the configuration considered here.

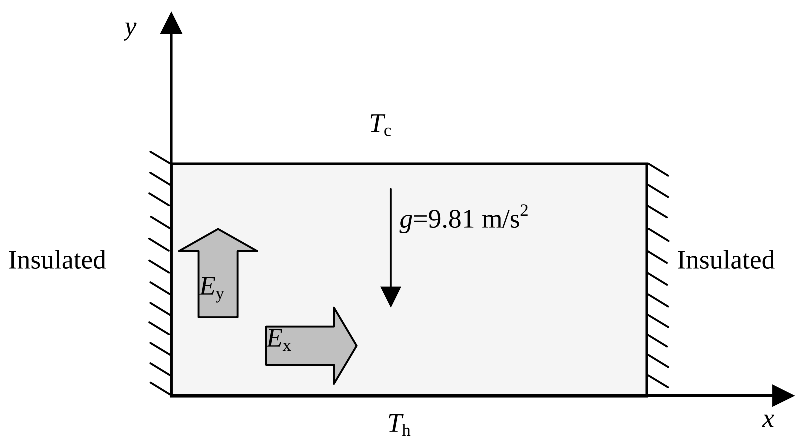

Figure 1. Geometry and boundary conditions.

The height and length of the cavity were equal to 33.33 mm and 66.67 mm, respectively. The left and right walls were kept thermally insulated. The bottom boundary was kept at a “hot” temperature while the top wall was kept at a “cold” temperature. A slightly triangular temperature profile was applied to the bottom wall in order to create a preferential direction for the fluid flow. For the test cases with Ra = 1.9x10^5 the temperature at the center of the bottom wall was 0.9 ^{o}C above its value at the corners, and for the test cases with Ra = 1.9x10^{4} the temperature at the center of the bottom wall was 0.09 ^{o}C above its value at the corners.

The left and bottom walls were subjected to unknown electric potential boundary conditions and the electric charged particles were supposed to enter the cavity from the locations where the electric potential was applied. The objective was to minimize [12] the natural convection effects by reducing the gradient of temperature along the *x* direction, thus trying to obtain a temperature profile similar to those obtained for pure conduction. The objective function to be minimized is then formulated as [12]

$$F = \sqrt{\frac{1}{\#cells}\sum_{i=1}^{\#cells}\left(\frac{\partial T_i}{\partial x_i}\right)^2} \tag{22}$$

The electric boundary conditions were inversely determined at six points equally spaced for the boundary where the electric field was applied and parameterized using B-splines [23] for the other points of such boundary.

In this paper we considered natural convection of Gallium Arsenide whose physical properties are summarized in Table 2.

The temperature difference T_h-T_c was set equal to 10 K, which gives a Rayleigh number of 1.9x10^{5}, where Ra is defined as

$$Ra = \frac{\rho\, C_P\, g\, \beta\left(T_h - T_c\right)L^3}{\nu\, K} \tag{23}$$

and L = 33.33 mm

Table 2. Physical properties for Gallium Arsenide

Property	**Value**	**Reference**
ρ_l	5710 kg m^{-3}	7
ρ_s	5196 kg m^{-3}	8
C_{Pl}	434 J kg^{-1} K^{-1}	7
C_{Ps}	416 J kg^{-1} K^{-1}	8
K_l	17.8 W m^{-1} K^{-1}	7
K_s	7 W m^{-1} K^{-1}	7
b_l	1 x 10^{-8} m^2 V^{-1}	24
b_s	1 x 10^{-14} m^2 V^{-1}	4
D_{el}	2.5 x 10^{-10} m^2 s^{-1}	25
D_{es}	2.5 x 10^{-16} m^2 s^{-1}	25
β_l	1.87 x 10^{-4} K^{-1}	7
β_s	1.87 x 10^{-4} K^{-1}	assumed
σ_l	8 x 10^5 W^{-1} m^{-1}	7
σ_s	3 x 10^4 W^{-1} m^{-1}	7
ε_0	8.854 x 10^{-12} kg m s^{-2} V^{-2}	25
L	726,000 J kg^{-1}	7
μ_l	2.79 x 10^{-3} kg m^{-1} s^{-1}	7
μ_s	2.79 x 10^2 kg m^{-1} s^{-1}	assumed
T_l	1511.005 K	4

T_s	1511 K	7

For the first test case, there was no phase change, since the “hot” and “cold” temperatures were above the melting temperature (T_h = 1525.995 K; T_c = 1515.995 K). Figures 2-4 show constant speed contours and constant temperature contours predicted for the first test case without any electric flux applied and no phase change for three different grid sizes.

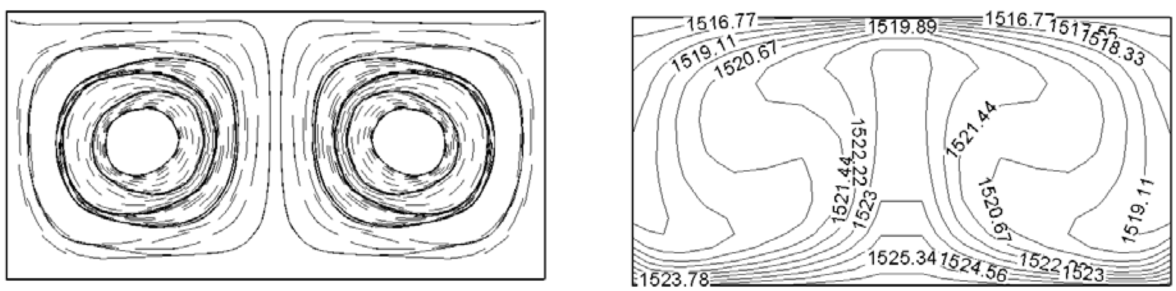

(a) (b)

Figure 2. Streamlines (a) and isotherms (b) with Ra = 1.9x10^5 and **E** = 0 (E_x = E_y = 0) for a grid with 20x20 cells.

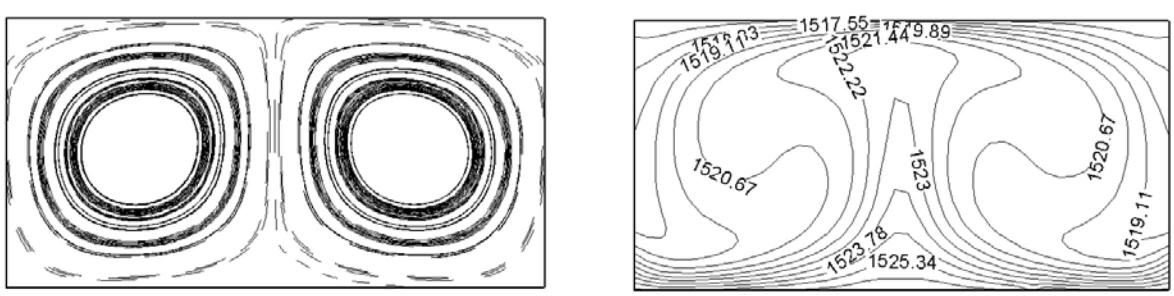

(a) (b)

Figure 3. Streamlines (a) and isotherms (b) with Ra = 1.9x10^5 and **E** = 0 (E_x = E_y = 0) for a grid with 40x40 cells.

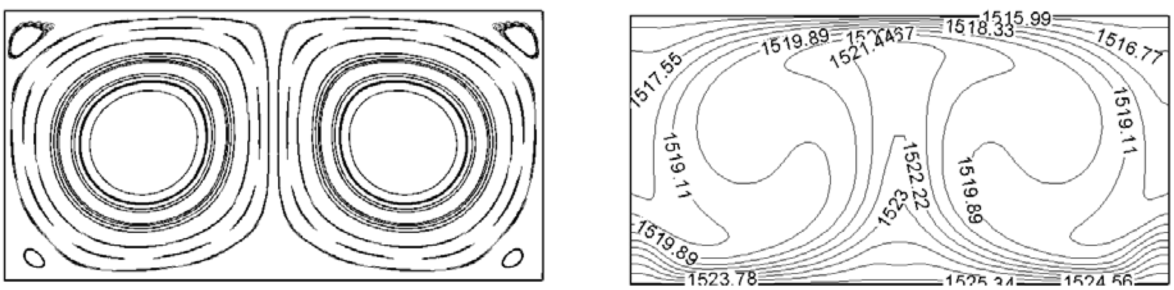

(a) (b)

Figure 4. Streamlines (a) and isotherms (b) with Ra = $1.9\text{x}10^5$ and **E** = 0 ($E_x = E_y = 0$) for a grid with 80x80 cells.

The computational times required to run the test case above with the three different grid sizes were 8 minutes, 43 minutes and 694 minutes on a Pentium IV 2.4 GHz machine for the 20x20, 40x40 and 80x80 grid sizes, respectively. Since a typical optimization job will require thousands of objective function evaluations, we chose the grid with 20x20 cells, so that it would be possible to run such optimization within a feasible computational time on a single processor personal computer. Thus, although the final results will not be fully converged, the concept that it is possible to control the natural convection phenomena by using externally applied electric fields could be demonstrated.

We tried to optimize the electric potential between the top and bottom walls, but no significant reduction of the objective function given by equation (22) was noticed. Then, we focused the optimization task on the electric potential between the right and left walls. In this process of optimization we fixed the maximum allowed value for the electric potential at 1000 volts, since higher values produced a very unstable flow-field. Figure 5 shows the optimized constant speed contours and temperature profiles using six points on the left boundary for the parameterization of the electric boundary condition. One can see that the gradients of temperature in the *x* direction are reduced close to the top and bottom walls. It is interesting to note that the temperature profile appears shifted to the left, when compared to Figure 2.

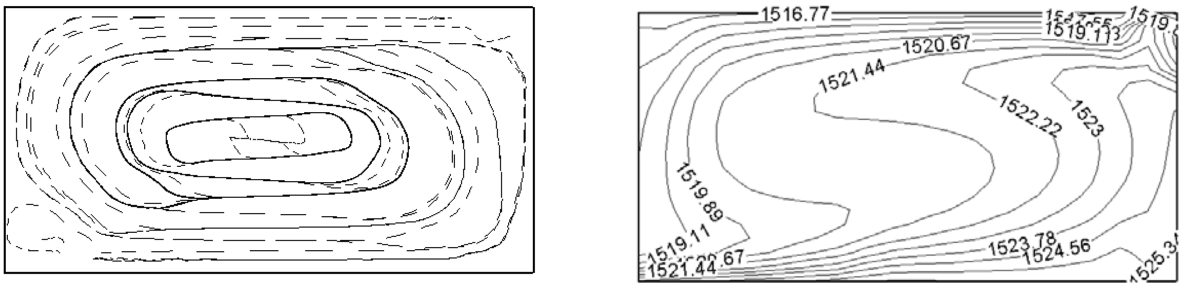

(a) (b)

Figure 5. Optimized streamlines (a) and isotherms (b) with Ra = $1.9\text{x}10^5$ and estimation of **E** at six points at $x = 0$.

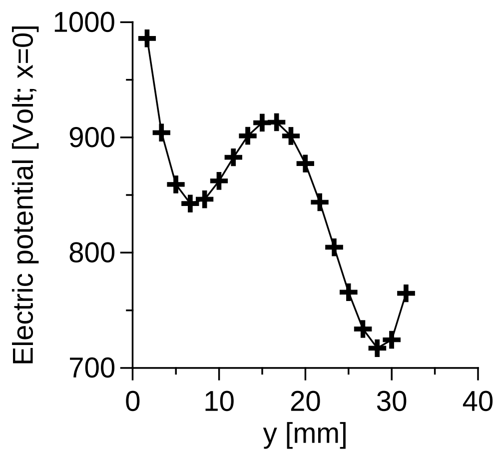

Figure 6. Electric boundary conditions at $x = 0$ with Ra = $1.9\text{x}10^5$ and estimation of **E** at six points.

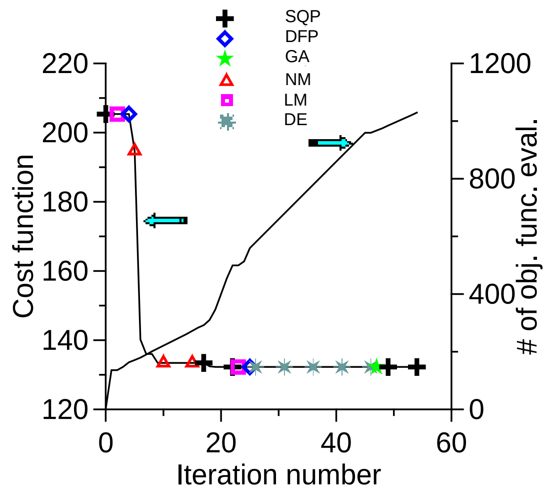

Figure 7. Convergence history for Ra = $1.9x10^5$ and estimation of **E** at six points at x = 0.

Figure 6 shows the optimized boundary conditions for x = 0 and Figure 7 shows the convergence history of the process where one can see that the Nelder-Mead (NM) module did almost all the work.

As a second test case, we tried to minimize the curvature of the isotherms in a solidifying process after a pre-specified time from the start of the solidifying process. Then, the eq. (22) was applied to the region between the solid and liquid phases. The temperature difference T_h-T_c was set equal to 10 K (T_h = 1515.995 K, T_c = 1505.995 K) and the length of the cavity was taken as the same as the previous test case. The solidus and liquidus temperatures were equal to 1511.0 K and 1511.005 K, respectively. Thus, a very thin mushy region exists between the phases.

Figures 8-9 show the constant speed contours and isotherms for this test case, predicted at 300 seconds (which is already the steady state solution) for two different grid sizes. The initial condition was set as $T_0 = T_h$. Then, the solidifying process starts at the top wall, where $T = T_c$.

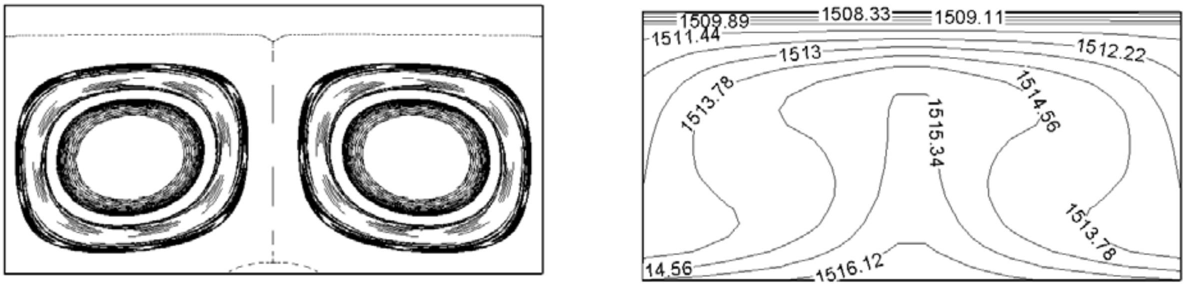

(a) (b)

Figure 8. Solidification case: Streamlines (a) and isotherms (b) with Ra = $1.9\text{x}10^5$ and **E** = 0 for a grid with 20x20 cells.

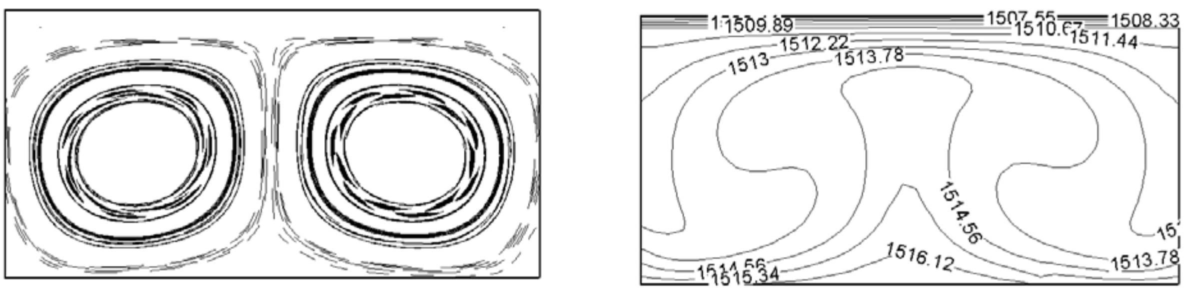

(a) (b)

Figure 9. Solidification case: Streamlines (a) and isotherms (b) with Ra = $1.9\text{x}10^5$ and **E** = 0 for a grid with 40x40 cells.

The computational times required to run the test case above with the two different grid sizes were 15 minutes and 116 minutes on a Pentium IV 2.4 GHz machine for the 20x20 and 40x40 grid sizes, respectively. Thus, for the same reason discussed above, we chose the 20x20 grid size to prove the concept proposed in this paper, even though the numerical results on this grid are not fully converged.

Figure 10 shows the optimized constant speed contours and isotherms using six points for the left boundary for the estimation of the electric boundary conditions. The boundary conditions at the other points on such boundary were interpolated using B-splines. One can see that the temperature profile appears “inverted” when compared to Figure 6. However, the flow-field starts to become highly unstable.

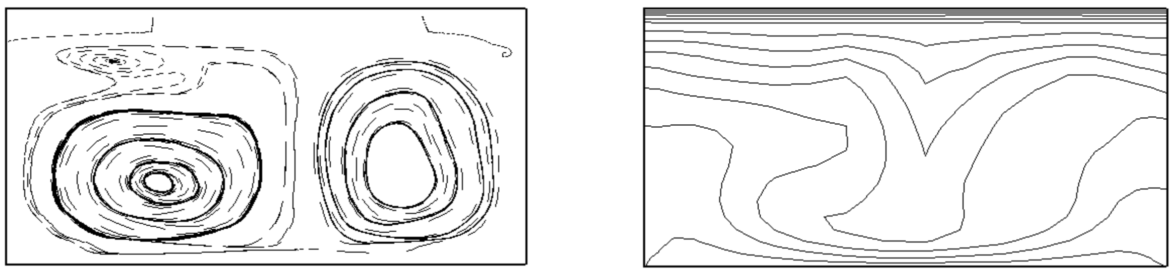

(a) (b)

Figure 10. Solidification case: Optimized streamlines (a) and isotherms (b) with Ra = 1.9×10^5 and estimation of **E** at six points at x = 0.

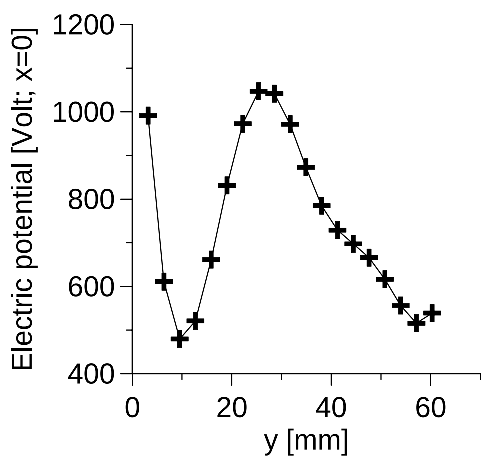

Figure 11. Solidification case: Electric boundary conditions at x = 0 with Ra = 1.9×10^5 and estimation of **E** at six points.

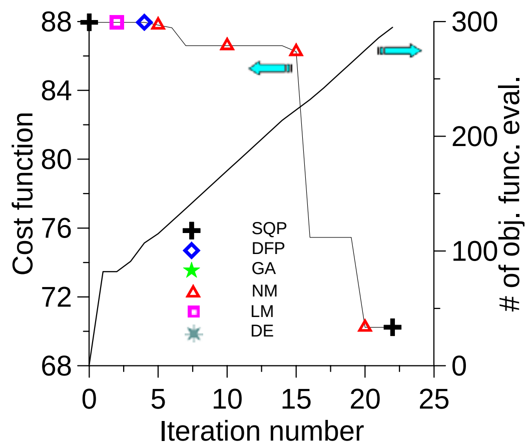

Figure 12. Solidification case: Convergence history for Ra = $1.9x10^5$ and estimation of **E** at six points at x = 0.

Figure 11 shows the optimized boundary condition for $x = 0$ and Figure 12 shows the convergence history of the optimization process where one can see that the Nelder-Mead (NM) module did almost all the work. The iterative process was forced to stop after 22 iterations due to the high computational cost involved when using a single processor personal computer. The computing time is significantly reduced and does not represent an issue when using inexpensive distributed parallel computers that are becoming readily available.

Due to the stability problems in the previous results, we applied the previous methodology to a test case with a lower Rayleigh number. Figures 13-15 shows the results obtained for three different grid sizes, without phase-change, for a Rayleigh number equal to $1.9x10^4$. In this case, the "hot" and "cold" temperatures were kept above the melting temperature (T_h = 1521.5 K; T_c = 1520.5 K). Note that the isotherms have a curvature weaker than those showed in Figures 2-4, for Ra = $1.9x10^5$.

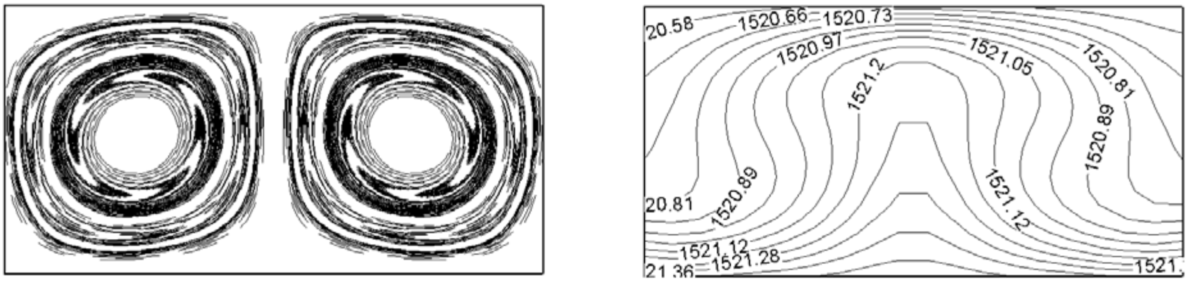

(a) (b)

Figure 13. Streamlines (a) and isotherms (b) with Ra = $1.9 x 10^4$ and **E** = 0 ($E_x = E_y = 0$) for a grid with 20x20 cells.

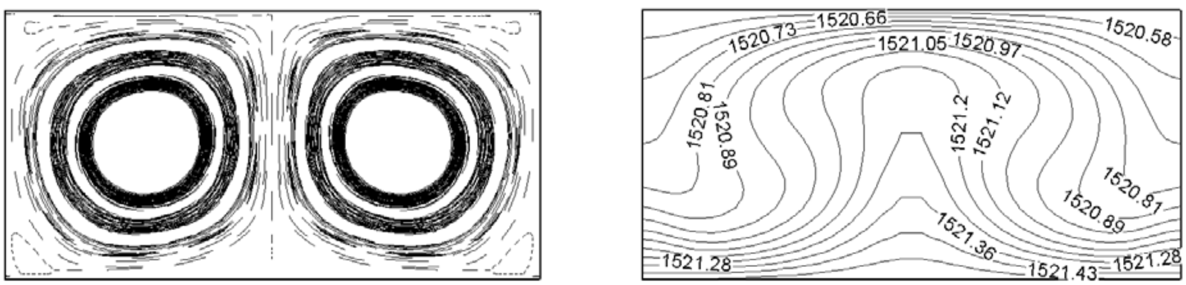

(a) (b)

Figure 14. Streamlines (a) and isotherms (b) with Ra = $1.9 x 10^4$ and **E** = 0 ($E_x = E_y = 0$) for a grid with 40x40 cells.

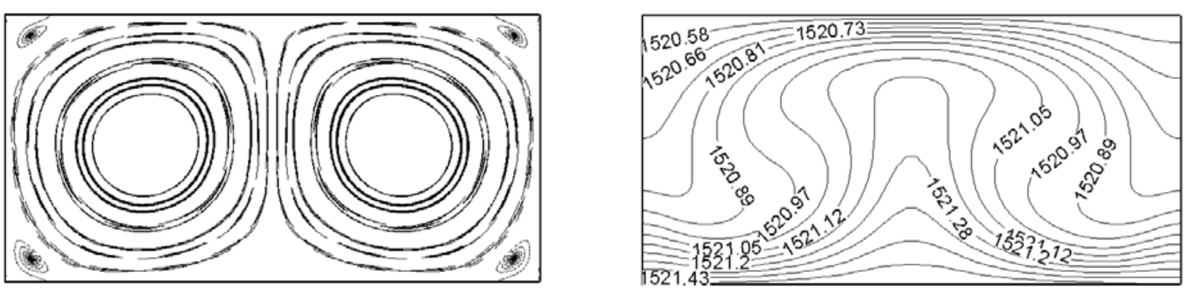

(a) (b)

Figure 15. Streamlines (a) and isotherms (b) with Ra = $1.9 x 10^4$ and **E** = 0 ($E_x = E_y = 0$) for a grid with 80x80 cells.

The computational times required to run the test-case above with the three different grid sizes were 9 minutes, 47 minutes and 892 minutes on a Pentium IV 2.4 GHz machine for the 20x20, 40x40 and 80x80 grid sizes, respectively. We again chose the 20x20 grid size, even if the numerical results on it are not fully converged, in order to minimize the computational time required by the optimization task.

Figure 16 shows the results obtained with an optimized electric potential in the *x*-direction, where one can see that the isotherms start to become horizontal. In fact, due to the body forces induced by the electric potential, the temperature profile is similar to those obtained if the gravity vector were acting in the horizontal direction. Figure 17 shows the optimized electric potential and figure 18 shows the convergence history, where the DFP and GA modules did all the work.

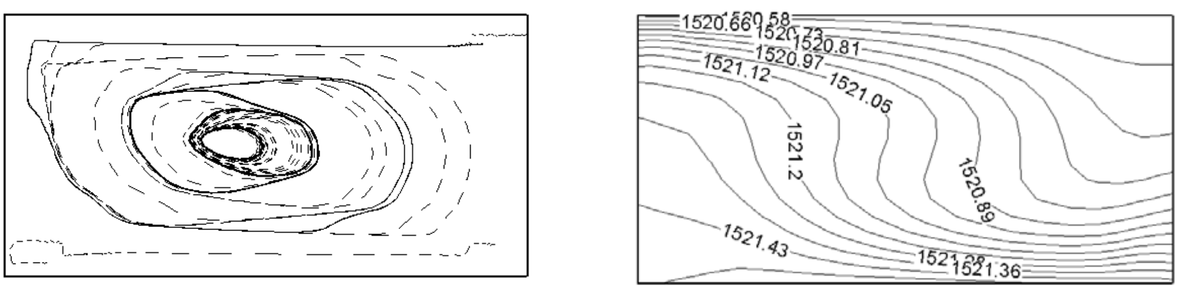

(a)   (b)

Figure 16. Optimized streamlines (a) and isotherms (b) with Ra = 1.9×10^4 and estimation of **E** at six points at $x = 0$.

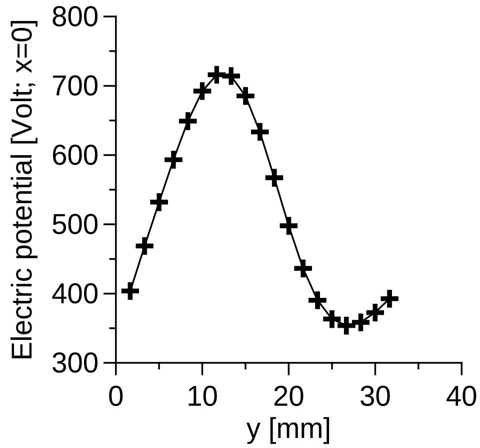

Figure 17. Electric boundary conditions at x = 0 with Ra = 1.9x10^4 and estimation of **E** at six points.

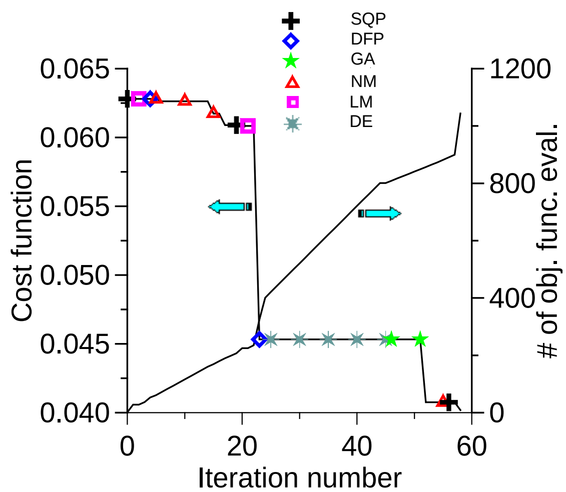

Figure 18. Convergence history for Ra = 1.9x10^4 and estimation of **E** at six points at x = 0.

For this test case with a lower Rayleigh number, we also tried to reduce the natural convection effects in the presence of phase-change. Figure 19 shows the results obtained for a Rayleigh number equal to 1.9x10^4 without any electric field applied for a 20x20 grid size, where the computational time was equal to 8 minutes on a Pentium IV 2.4 GHz machine. In this case, the “hot” and “cold” temperatures were equal to 1510.5 K and 1511.5 K, respectively. Note that the isotherms have a curvature weaker than those in Figure 8-9, for Ra = $1.9\text{x}10^5$.

Figure 20 shows the results obtained with an optimized electric potential acting in the horizontal direction. Note that the isotherms are smoother than those in Figure 19 for a case without any electric field applied. It is interesting to note that the velocity profile is very unstable, even for this case with a low Rayleigh number.

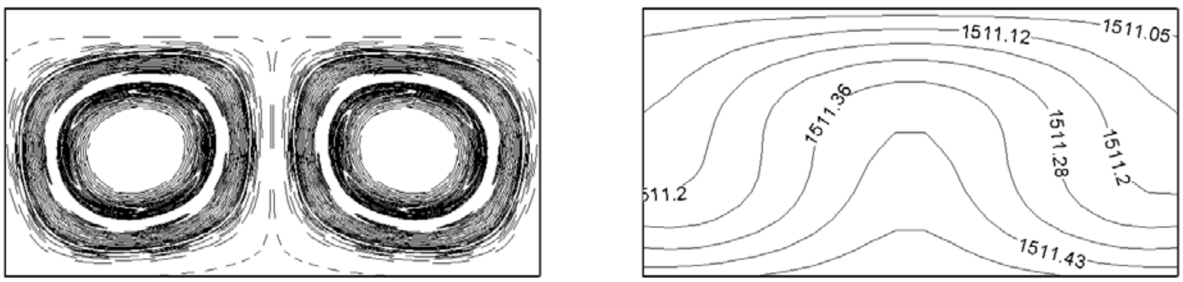

(a) (b)

Figure 19. Solidification case: Streamlines (a) and isotherms (b) with Ra = $1.9\text{x}10^4$ and **E** = 0 for a grid with 20x20 cells.

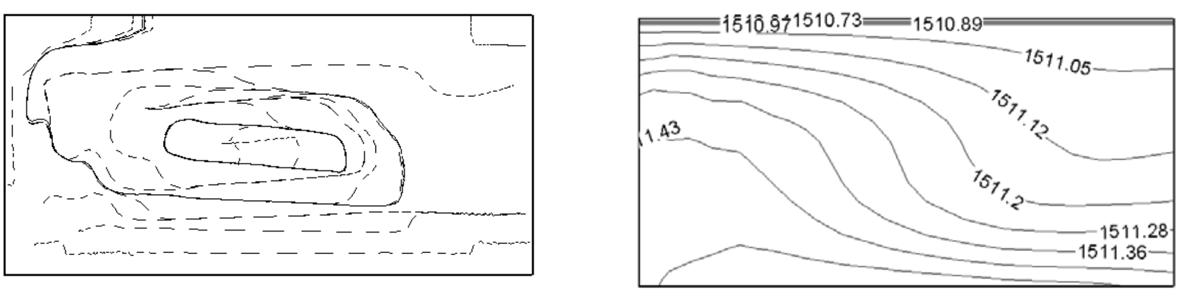

(a) (b)

Figure 20. Solidification case: Optimized streamlines (a) and isotherms (b) with Ra = $1.9\text{x}10^4$ and estimation of **E** at six points at x = 0.

Figure 21 shows the optimized electric potential and figure 22 shows the convergence history for the hybrid optimizer. Note that the differential evolution (DE) module did almost all the work for this test case.

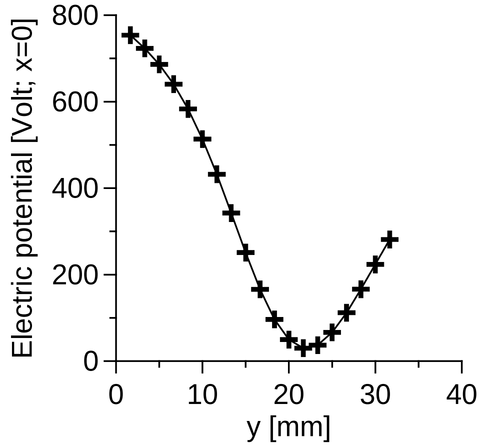

Figure 21. Solidification case: Electric boundary conditions at x = 0 with Ra = 1.9x10^4 and estimation of **E** at six points.

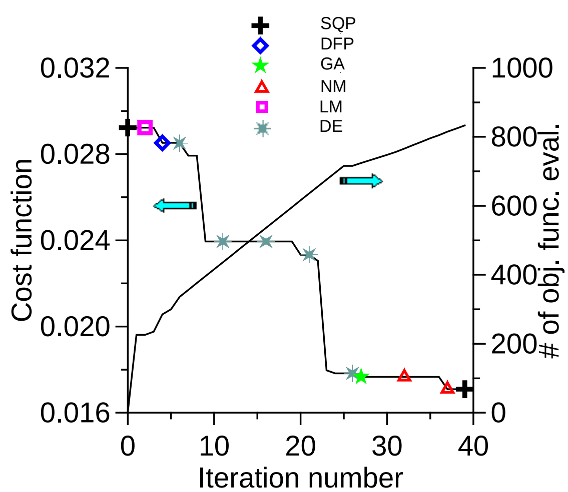

Figure 22. Solidification case: Convergence history for Ra = 1.9×10^4 and estimation of **E** at six points at $x = 0$.

CONCLUSIONS

In this paper we showed the results of a time-accurate EHD code that is capable of dealing with phase change problems. The ability to minimize the natural convection effects in problems with and without phase change was demonstrated by utilizing an optimized distribution of electric field along the boundaries of a solidification container for the purpose of controlling the solidification process. A hybrid constrained optimization algorithm was used in reducing such natural convection effects.

However, when space-varying electric potentials were applied, the fluid-flow started to become highly unstable. For cases where the electric potential was constant along certain wall, such instability did not occur. Further investigations concerning the stability of this type of fluid flow are necessary. Also, it is necessary to repeat the analysis presented in this paper by using more sophisticated mathematical models of solidification and by using a more refined grid. Actually, the instabilities presented in the velocity profiles could be due to the lack of convergence because of the very coarse grid used in these computations. However, the concept that it is possible to control the fluid flow by the means of an externally applied electric field has been adequately demonstrated.

AKNOWLEDGEMENTS

The first author is grateful for the postdoctoral fellowship received from University of Texas at Arlington and from CNPq and CAPES, two Brazilian agencies for scientific and technological development.

The second author is grateful for the partial support provided for this research from the grant NSF DMS-0073698 administered through the Computational Mathematics program.

REFERENCES

1. Dulikravich, G. S. Electro-Magneto-Hydrodynamics and Solidification; Chapter no. 9 in *Advances in Flow and Rheology of Non-Newtonian Fluids*, Part B; Siginer, D. A., De Kee, D. and Chhabra, R. P., Eds., Rheology Series, 8; Elsevier Publishers, **1999,** 677-716.

2. Dulikravich, G. S. and Lynn, S. R. Unified Electro-Magneto-Fluid Dynamics (EMFD): Introductory Concepts. *International Journal of Non-Linear Mechanics*, **1997**, 32 (5), 913-922.

3. Dulikravich, G. S. and Lynn, S. R. Unified Electro-Magneto-Fluid Dynamics (EMFD): A Survey of Mathematical Models. *International Journal of Non-Linear Mechanics*, **1997**, 32 (5), 923-932.

4. Dulikravich, G. S., Ahuja, V. and Lee, S. Modeling of Dielectric Fluid Solidification with Charged Particles in Electric Fields and Reduced Gravity. *Numerical Heat Transfer, Part B*, **1994**, 25, 357-373.

5. Dulikravich, G. S., Martin, T. J., Dennis, B. H. and Foster, N. F. Multidisciplinary Hybrid Constrained GA Optimization; Chapter 12 in *EUROGEN'99 - Evolutionary Algorithms in Engineering and Computer Science: Recent Advances and Industrial Applications*; Miettinen, K., Makela, M. M., Neittaanmaki, P. and Periaux, J., Eds.; John Wiley & Sons: Jyvaskyla, Finland, May 30 - June 3, **1999**, 233-259.

6. Rappaz, M. Modelling of Microstructure Formation in Solidification Process. *International Materials Reviews*, **1989**, 34 (3), 93-123.

7. Sabhapathy, P. and Salcudean, M. E. Numerical Study of Flow and Heat Transfer in LEC Growth of GaAs with an Axial Magnetic Field. *Journal of Crystal Growth*, **1990**, 104, 371-388.

8. Brodsky, M. H., *Properties of Gallium Arsenide*, 2nd ed., INSPEC, EMIS Datareview Series, no. 2, **1990**.

9. Dulikravich, G. S., Ahuja, V. and Lee, S. Modeling Three-Dimensional Solidification With Magnetic Fields and Reduced Gravity. *International Journal of Heat and Mass Transfer*, **1994**, 37 (5), 837-853.

10. Dennis, B. H. and Dulikravich, G. S. Magnetic Field Suppression of Melt Flow in Crystal Growth. *International Journal of Heat & Fluid Flow*, **2002**, 23 (3), 269-277.

11. Colaço, M. J., Dulikravich, G. S. and Martin, T. J. Reducing Convection Effects in Solidification by Applying Magnetic Fields Having Optimized Intensity Distribution. ASME paper HT2003-47308, ASME Summer Heat Transfer Conference**,** Las Vegas, NV, July 21-23, **2003**.

12. Dulikravich, G. S., Colaço, M. J., Martin, T. J. and Lee, S. Optimization of Intensities and Orientations of Magnets Controlling Melt Flow During Solidification. *J. of Materials and Manufacturing Processes*, **2004,** 19 (3).

13. Dulikravich, G. S., Colaco, M., Martin, T. J. and Lee, S. Magnetized Fiber Orientation and Concentration Control in Solidifying Composites. *Journal of Composite Materials*, **2003**, 37 (15) 1351-1366.

14. Meir, A. J., Schmidt, P. G., Bakhtiyarov, S. I. and Overfelt, R. A. Velocity, Potential, and

Temperature Distributions in Molten Metals During Electromagnetic Stirring, Part II: Numerical Simulations, *Symp. on Rheology and Fluid Mechanics of Nonlinear Materials*, ASME IMECE’99, (ed: D. A. Siginer), Nashville, TN, Nov. 14-19, 1999, ASME FED-Vol. 249, pp. 97-104, **1999**.

15. Voller, V. R., Brent, A. D. and Prakash, C. The Modeling of Heat, Mass and Solute Transport in Solidification Systems. *International J. Heat Mass Transfer*, **1989**, 32, 1719-1731.

16. Chakraborty, S. and Dutta, P. A Generalized Formulation for Evaluation of Latent Heat Functions in Enthalpy-Based Macroscopic Models for Convection-Diffusion Phase Change Processes. *Metallurgical and Materials Transaction B,* **2001**, 32b, 562-564.

17. Chakraborty, S. and Dutta, P. The Effect of Solutal Undercooling on Double-Diffusive Convection and Macrosegregation During Binary Alloy Solidification: A Numerical Investigation**.** *International J. for Numerical Methods in Fluids*, **2002,** 38 (9) 895-917.

18. Chakraborty, S., Chakraborty, N., Kumar, P. and Dutta, P. Studies on Turbulent Momentum, Heat and Species Transport During Binary Alloy Solidification in a Top-Cooled Rectangular Cavity. **2002**, *International J. for Heat and Mass Transfer*, 38 (8) 1115-1137.

19. Van Doormal, J. P. and Raithby, G. D. Enhancements of the SIMPLE Method for Predicting Incompressible Fluid Flow. *Numerical Heat Transfer*, **1984**, Vol. 7, 147-163.

20. Raithby, G. D. and Torrance, K. E. Upstream-Weighted Differencing Schemes and Their Application to Elliptic Problems Involving Fluid Flow. *Computers & Fluids*, **1974**, 2, 191-206.

21. Press, W. H., Flannery, B. P., Teukolsky, S. A. and Vetterling, W. T., *Numerical Recipes in Fortran*, Cambridge University Press, **1992**.

22. Colaço, M. J., Orlande, H. R. B., Dulikravich, G. S. and Rodrigues, F. A. A Comparison of Two Solution Techniques for the Inverse Problem of Simultaneously Estimating the Spatial Variations of Diffusion Coefficients and Source Terms. ASME paper IMECE2003-42058, Washington, DC, November 16-21, **2003**.

23. Barsky, B. A. *Computer Graphics and Geometric Modeling Using Beta-Splines*; Springer-Verlag: Berlin, Germany, **1988**.

24. Saville, D. A. and Palusinski, O. A. Theory of Electrophoretic Separation. *AIChE Journal*, **1986**, 32 (2), 207-214.

25. Eringen, A. C. and Maugin, G. A. *Electrodynamics of Continua II – Fluids and Complex Media*; Springer-Verlag: New York, **1990**.

Keywords:

solidification, electrohydrodynamics, numerical methods, optimization, manufacturing processes, finite volume method.